



# La doping and coating enabled by one-step method for high performance $\text{Li}_{1.2}\text{Mn}_{0.54}\text{Ni}_{0.13}\text{Co}_{0.13}\text{O}_2$ Li-rich cathode

Yongqing Tang<sup>1</sup> · Xiang Han<sup>2</sup> · Weishan Zhang<sup>1</sup> · Yongjun He<sup>1</sup>

Received: 25 February 2020 / Revised: 27 March 2020 / Accepted: 30 March 2020 / Published online: 8 May 2020  
© Springer-Verlag GmbH Germany, part of Springer Nature 2020

## Abstract

The poor cycle performance and rate capability limit the wide application of lithium-rich cathode materials. Herein, we propose a one-step method for  $\text{La}^{3+}$  doping and  $\text{LaMnO}_3$  coating by co-precipitation to improve the electrochemical performance of the  $\text{Li}_{1.2}\text{Mn}_{0.54}\text{Ni}_{0.13}\text{Co}_{0.13}\text{O}_2$ . XRD, EDS of the cross section, and TEM successfully confirm that  $\text{La}^{3+}$  is doped into the material structure and  $\text{LaMnO}_3$  is uniformly coated on the surface of  $\text{Li}_{1.2}\text{Mn}_{0.54}\text{Ni}_{0.13}\text{Co}_{0.13}\text{O}_2$ . The  $\text{Li}_{1.2}\text{Mn}_{0.54-x}\text{Ni}_{0.13}\text{Co}_{0.13}\text{La}_x\text{O}_2$  ( $x = 0.03$ ) (abbreviated as LR-NMC@0.03) sample delivers a discharge capacity as high as  $248.1 \text{ mAh g}^{-1}$  at 1C compared with that of  $212.3 \text{ mAh g}^{-1}$  for the pristine sample. More importantly, the capacity retention for the LR-NMC@0.03 sample after 100 cycles can reach 92.5%, which is significantly higher than that of 76.8% for the pristine sample. The better rate capability and cyclic performance of the LR-NMC@0.03 sample are attributed to the double strengthening effect by both the  $\text{La}^{3+}$  doping and  $\text{LaMnO}_3$  coating with better host structural and surface stability.

**Keywords** Lithium-rich ·  $\text{La}^{3+}$  doping ·  $\text{LaMnO}_3$  coating · Lithium-ion batteries

## Introduction

With continuous consumption of traditional non-renewable energy, new energy resources have attracted more and more researchers' attention. Lithium-ion batteries have the advantages of high specific energy, low self-discharge rate, long cycle life, no memory effect and low environmental pollution. They have become important energy storage devices in the fields of renewable energy, smart grid, and new energy automotive technology [1–4]. Since  $\text{LiCoO}_2$  (LCO) was commercialized and marketed by Sony in 1991, it has been widely used in consumer electronics products. Nevertheless, its inherent low energy density and expensive raw materials limit its application in power vehicles, for example, the pure electric vehicles [5]. Owing to the continuous efforts of scientists, cathode materials such as  $\text{Li}[\text{Ni}_x\text{Co}_y\text{Mn}_{1-x-y}]\text{O}_2$  [6–10],  $\text{LiFePO}_4$  [11, 12], and  $\text{LiMn}_2\text{O}_4$  [13, 14] have been

continuously developed. Compared with LCO, although they have lower cost, they still cannot meet the consumers for high-capacity cathode materials [1, 2].

In recent years, a layered transition metal oxide cathode material with chemical formula of  $z\text{Li}_2\text{MO}_3 \cdot (1-z)\text{LiMO}_2$  ( $0 < z < 1$ ,  $M = \text{Mn}_{0.5}\text{Ni}_{0.5}$ ,  $\text{Mn}_x\text{Ni}_y\text{Co}_{(1-x-y)}$ ,  $0 < x, y < 1$ ,  $0 < x + y < 1$ ) has attracted many researchers' attention. The Li-rich Mn-based layered oxide, typical representative  $\text{Li}_{1.2}\text{Mn}_{0.54}\text{Ni}_{0.13}\text{Co}_{0.13}\text{O}_2$ , has a high theoretical specific capacity ( $> 250 \text{ mAh/g}$ ) and low cost, which is regarded as the most promising cathode materials for the next-generation Li-ion batteries. However, the low initial irreversible capacity, poor cycle performance, poor rate capability, and potential dropping limit its further application [15–20].

So far, most of the current research work focuses on simple doping and coating to improve the inherent defects of lithium-rich cathode materials. Different modifications of lithium-rich cathode were carried out in early research works, for example, the  $\text{Mg}^{2+}$  [21],  $\text{Al}^{3+}$  [22], and  $\text{Cr}^{3+}$  [23] doping and  $\text{Al}_2\text{O}_3$  [24],  $\text{ZnO}$  [25], and  $\text{ZrO}_2$  [26] coating. Although these works have improved the electrochemical performance of lithium-rich cathode materials to some extent, there is still much room for improvement. As known to us, the structure of the lithium-rich cathode material will collapse after being charged and discharged, and it is easily eroded by the electrolyte [27].

✉ Yongqing Tang  
tangyongqing1988@sina.cn

<sup>1</sup> Sichuan Police College, Luzhou 646000, China

<sup>2</sup> College of Materials Science and Engineering, Nanjing Forestry University, Nanjing 210037, China

Simple doping can stabilize the structure of lithium-rich cathode materials to some extent; however, the erosion of the material by the electrolyte is difficult to be avoided. And the simple coating can suppress the side reaction of between the electrolyte and the lithium-rich cathode materials to some extent, but it is also difficult to maintain the structural stability in long charge-discharge cycles.

In order to improve the electrochemical performance of lithium-rich cathode more effectively, here we propose a one-step method for doping and coating. Super heterovalent cation 'La<sup>3+</sup>' was selected as the doping element to replace 'Mn<sup>4+</sup>' in layered lithium-rich cathode materials Li<sub>1.2</sub>Mn<sub>0.54</sub>Ni<sub>0.13</sub>Co<sub>0.13</sub>O<sub>2</sub>. The binding energy of La–O bond is higher than that of Ni–O or Mn–O bond. The Gibbs free energy of formation of La<sub>2</sub>O<sub>3</sub>, MnO<sub>2</sub> and NiO is –1763.54 kJ mol<sup>–1</sup>, –465.1 kJ mol<sup>–1</sup>, and –211.7 kJ mol<sup>–1</sup>, respectively. Based on the above analysis, 'La<sup>3+</sup>' doping can effectively improve the stability of layered lithium-rich cathode materials. Due to the radius of the trivalent, La-ion is obviously larger than that of the tetravalent Mn-ion [28]; as a result, such a huge ion doping into the layered structure will effectively broaden the lithium-ion channel in the lattice and further improve the rate performance of the lithium-rich cathode material. It is worth mentioning that due to the heterovalent doping, the doping element 'La<sup>3+</sup>' cannot be completely entered into the material structure; instead, a part of the undoping 'La<sup>3+</sup>' ion is coated on the surface of the lithium-rich cathode material in the form of La compound. Thus, the application of heterovalent 'La<sup>3+</sup>' ion in the modification of lithium-rich cathode materials can stabilize the layered structure of the material. At the same time, the La-containing compound formed on the surface of the material can effectively prevent the electrolyte from eroding the material, so as to effectively improve the electrochemical performance of lithium-rich cathode materials.

## Experimental

### Materials synthesis

Carbonate co-precipitation method was adopted to synthesis La-doping Li-rich precursor of Li<sub>1.2</sub>Mn<sub>0.54-x</sub>Ni<sub>0.13</sub>Co<sub>0.13</sub>La<sub>x</sub>O<sub>2</sub> (x = 0, 0.01, 0.03, 0.05) lithium-rich cathode materials. According to the stoichiometric ratio of Li<sub>1.2</sub>Mn<sub>0.54-x</sub>Ni<sub>0.13</sub>Co<sub>0.13</sub>La<sub>x</sub>O<sub>2</sub> (x = 0, 0.01, 0.03, 0.05), MnSO<sub>4</sub>·H<sub>2</sub>O, CoSO<sub>4</sub>·7H<sub>2</sub>O, NiSO<sub>4</sub>·6H<sub>2</sub>O, and La (NO<sub>3</sub>)<sub>3</sub>·6H<sub>2</sub>O of different proportions were dissolved in deionized water to prepare a 2 mol/L sulfate mixed solution. Na<sub>2</sub>CO<sub>3</sub> was selected as the precipitant and dissolved in deionized water to form a 2 mol/L Na<sub>2</sub>CO<sub>3</sub> aqueous solution. At the same time, appropriate amount of NH<sub>3</sub>·H<sub>2</sub>O as a complexing agent was added to the Na<sub>2</sub>CO<sub>3</sub> aqueous solution. The above

two mixed solutions were dropped into the container simultaneously in the process of continuous stirring with the speed of 1000 rpm/min. During the reaction, the pH in the solution was controlled by NH<sub>3</sub>·H<sub>2</sub>O, and the pH was always maintained at about 7.8. In order to obtain precursors with better morphology, the reaction temperature and time were strictly maintained at 60 °C and 10 h, respectively. After aging for 12 h and stirring, filtering, and vacuum drying for 12 h, Li-rich precursor by La doping with spherical morphology can be obtained. Considering that lithium will volatilize during the sintering process, 5at% excess of lithium carbonate was added to the precursor. Li<sub>2</sub>CO<sub>3</sub> was mixed with the precursor uniformly by ball mill, and then the above mixture was first calcined in a muffle furnace at 550 °C for 6 h and subsequently calcined at 900 °C for 12 h to obtain lithium-rich manganese-based cathode materials doped with different La content.

### Characterization

The morphology of the samples and the distribution of the elements were observed by the scanning electron microscopy equipped with an energy dispersive (SEM/EDS, Sigma-H, Carl Zeiss Germany). X-ray diffraction (XRD, Rigaku IV, Nippon Science Corporation) was applied to analysis the samples' phase composition and structure. The coating morphology on the particle surface was adopted by transmission electron microscopy (TEM, Philips Tecnai F30).

### Electrochemical test

The electrochemical properties of the pristine and modified materials were tested by the CR2032-type coin cells. The average mass loading of the active materials is 2.5 mg cm<sup>–2</sup>. NMP (N-methylpyrrolidone) was used as a dispersant during the electrode sheet. The cathode material, PVDF (polyvinylidene fluoride), and acetylene black were mixed uniformly with a mass ratio of 80:10:10, and then the mixed slurry was evenly coated on the aluminum foil. The prepared cathode sheets were dried in a vacuum drying oven at 90 °C for 12 h. The coin cells were assembled in a fully dry Ar-filled glove box with water content and oxygen content lower than 0.1 ppm. Lithium metal sheets were used as the negative electrode, Celgard2400 microporous polypropylene membrane was used as the separator, and the electrolyte was 1 mol/L LiPF<sub>6</sub> dissolved in 1:1 (V/V) vinyl carbonate (EC) and dimethyl carbonate (DMC). LAND (CT2001A) battery tester was used to test the galvanostatic charge-discharge. The voltage range was 2.0~4.6 V. AC impedance test was conducted by CHI660B electrochemical workstation with an amplitude of 10 mV from 100 KHz to 0.1 Hz.

## Results and discussion

Figure 1 shows the XRD diffraction patterns of  $\text{Li}_{1.2}\text{Mn}_{0.54-x}\text{Ni}_{0.13}\text{Co}_{0.13}\text{La}_x\text{O}_2$  ( $x = 0, 0.01, 0.03, 0.05$ ) Li-rich cathodes. As shown in Fig. 1, all  $\text{La}^{3+}$ -doping samples show the characteristic diffraction peaks of layered lithium-rich manganese-based cathode materials. The pristine and  $\text{La}^{3+}$  modified samples present a layered R-3m  $\text{LiCoO}_2$  like  $\alpha\text{-NaFeO}_2$  standard characteristic peak. All samples show weak diffraction peaks between  $20^\circ$  and  $25^\circ$ , which is mainly due to the existence of the material composition  $\text{Li}_2\text{MnO}_3$  in the transition metal layer, resulting in the characteristic signs of  $\text{LiMn}_6$ -type superlattice [29, 30]. The (006)/(012) and (018)/(110) characteristic peak pairs of all samples are obvious, which shows that all the samples have good crystallinity. With the increase of  $\text{La}^{3+}$  doping content, the peak of the main phase has not changed significantly, and the obvious characteristic peaks of the layered lithium-rich manganese-based cathode material are still maintained.

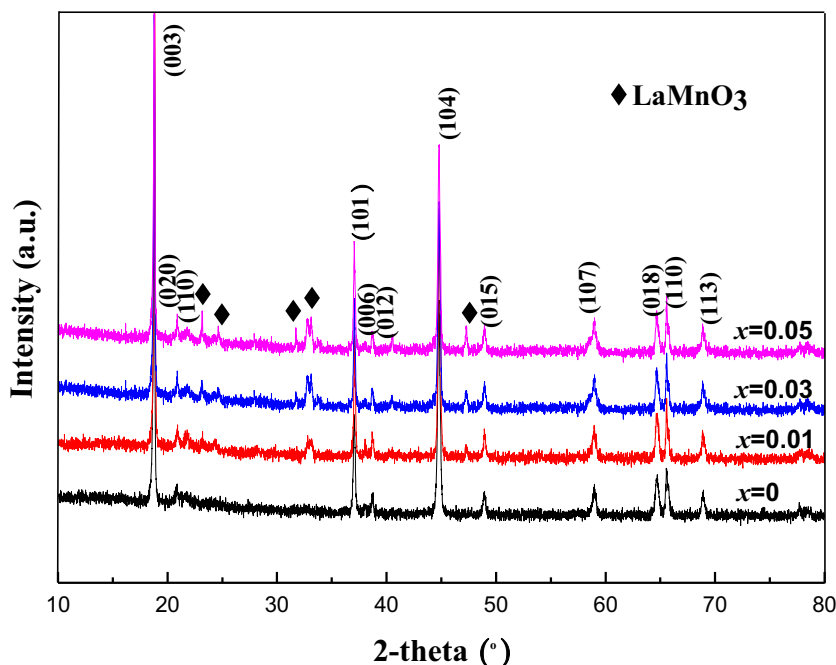
The previous research results show that the change of the lattice constant of the material can confirm whether the doping element has entered into the lattice of the material [31]. Jade software was used to calculate the lattice constant and (003)/(104) peak intensity ratio of the samples. The calculation results are shown in Table 1. It can be seen from the data in Table 1 that the lattice constants  $a$  and  $c$  of the  $\text{La}^{3+}$  modified samples are larger than those of unmodified samples. Therefore, it can be concluded that  $\text{La}^{3+}$  ion has been successfully diffused to the lithium-rich material structure.  $\text{La}^{3+}$  doping broadens the lithium intercalation diffusion channel of the cathode electrode material, which is mainly due to  $\text{La}^{3+}$

**Table 1** Crystal structure parameters of  $\text{Li}_{1.2}\text{Mn}_{0.54-x}\text{Ni}_{0.13}\text{Co}_{0.13}\text{La}_x\text{O}_2$  ( $x = 0, 0.01, 0.03, 0.05$ ) Li-rich cathodes

Sample ( $x$ )	$a/\text{\AA}$	$c/\text{\AA}$	$c/a$	$I(003)/I(104)$
0.00	2.8527	14.2364	4.9905	1.51
0.01	2.8531	14.2458	4.9931	1.65
0.03	2.8545	14.2705	4.9993	1.76
0.05	2.8538	14.2539	4.9947	1.66

ion radius is larger than  $\text{Mn}^{4+}$  ion radius. The result is similar to those reported in the research [32, 33]. It is worth noting that as the doping amount of La increases, the lattice constant of the sample does not increase linearly. This may be due to the strong binding force between La and O. When the doping amount reaches a certain level, the strong binding force with O shrinks the interlayer spacing [28]. In general, the lattice constant  $c/a$  can be used as an index for evaluating the characteristics of layered structure materials. The higher the  $c/a$ , the better the layered structure characteristics. It can be seen from the data in Table 1 that the  $c/a$  value of  $\text{La}^{3+}$ -doping samples are higher than those of undoping samples, indicating that  $\text{La}^{3+}$ -doping samples have better layered structure characteristics than undoping samples. In addition, the peak intensity ratio of  $I(003)/I(104)$  is related to the mixed arrangement degree of  $\text{Li}^+$  and  $\text{Ni}^{2+}$  cations in the layered structure of the cathode material. All  $\text{La}^{3+}$ -doping samples have higher  $I(003)/I(104)$  peak intensity ratios than the undoping samples. Therefore, it can be concluded that the mixed arrangement of  $\text{Li}^+$  and  $\text{Ni}^{2+}$  cations in the layered structure of the material can be inhibited by  $\text{La}^{3+}$  doping to a certain extent.

**Fig. 1** XRD patterns of  $\text{Li}_{1.2}\text{Mn}_{0.54-x}\text{Ni}_{0.13}\text{Co}_{0.13}\text{La}_x\text{O}_2$  ( $x = 0, 0.01, 0.03, 0.05$ ) Li-rich cathodes



It should be noted that  $\text{LaMnO}_3$  second phase occurs in the XRD pattern of the La-doping samples shown in Fig. 1. Furthermore, as the amount of La-doping increases, the peak intensity of  $\text{LaMnO}_3$  second phase increases. The formation of  $\text{LaMnO}_3$  second phase can be ascribed to the reason that the  $\text{La}^{3+}$  ions were not fully doped into the layered structure of the lithium-rich cathode material. Combined with the abovementioned XRD structural analysis of La-doping, to further prove that  $\text{La}^{3+}$  ion has been entered the lithium-rich material structure and clarify the existence form of  $\text{LaMnO}_3$  second phase, the cross-section EDS analysis was applied in this paper. Figure 2a presents EDS analysis results of LR-NMC@0.03 Li-rich cathodes' cross section. In the experiment, the data were collected in the diameter direction and on the surface of the lithium-rich cathode particle at a distance about 1  $\mu\text{m}$ . The typical EDS spectrum shown in Fig. 2b was established to demonstrate the presence of Mn, Co, Ni, O, and La. Experimental test results shown in Fig. 2c demonstrate

that the La contents from point 1 to point 5, i.e., the interior to the surface of the LR-NMC@0.03 particle, are 0.46, 0.53, 0.48, 0.61, and 0.87at%, respectively. As shown in Fig. 2c, the variety trend of the La content from the interior to the surface of the particle can be clearly seen. It should be noted that the particle interior had been detected and the La contents were all lower than the theoretical La content (0.75at%), revealing that  $\text{La}^{3+}$  ion has been doped into the layered structure of the lithium-rich cathode material successfully. This result is consistent with the conclusion of the aforementioned XRD analysis.

One can find that the surface La contents of the LR-NMC@0.03 particle are significantly higher than those of the interior. Figure 2d exhibits La content distribution curve of the particle surface; as shown in Fig. 2d, La contents of the particle surface vary little, and the calculation results show that the average La content of the particle surface is about 0.90at%. Combined with the  $\text{LaMnO}_3$  second phase appeared

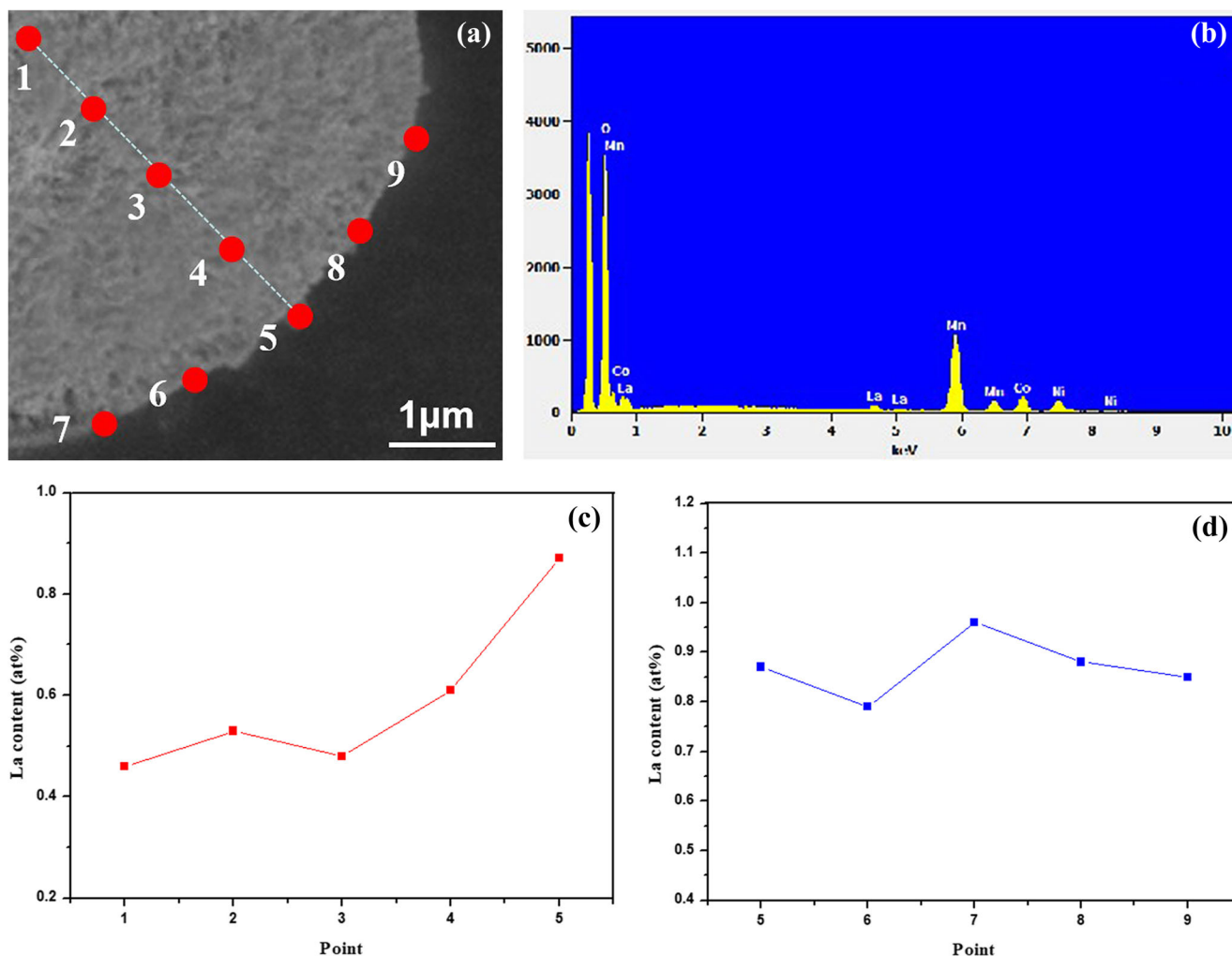


**Fig. 2** SEM image of LR-NMC@0.03 Li-rich cathode cross section exhibiting the areas marked with the red dots where the point EDS analyses were performed, for **a** SEM image of cross section. **b** Representative

EDS test spectrum. **c** La content from the interior to the surface of the cross section. **d** La content on the surface of cathode particle

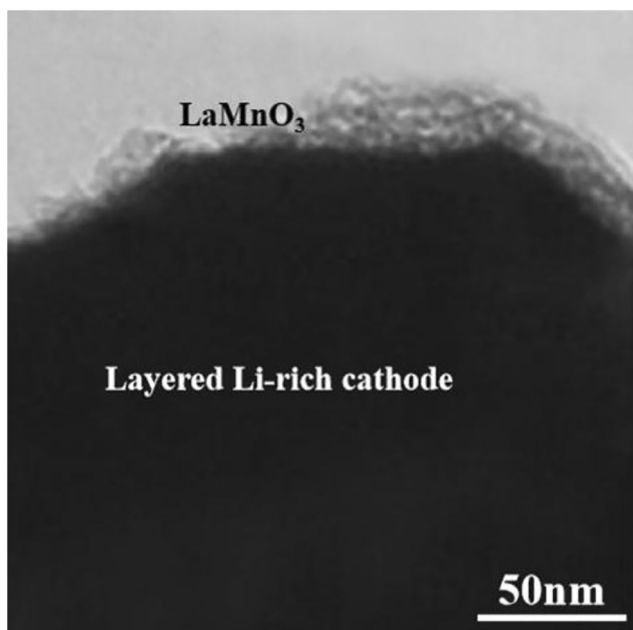


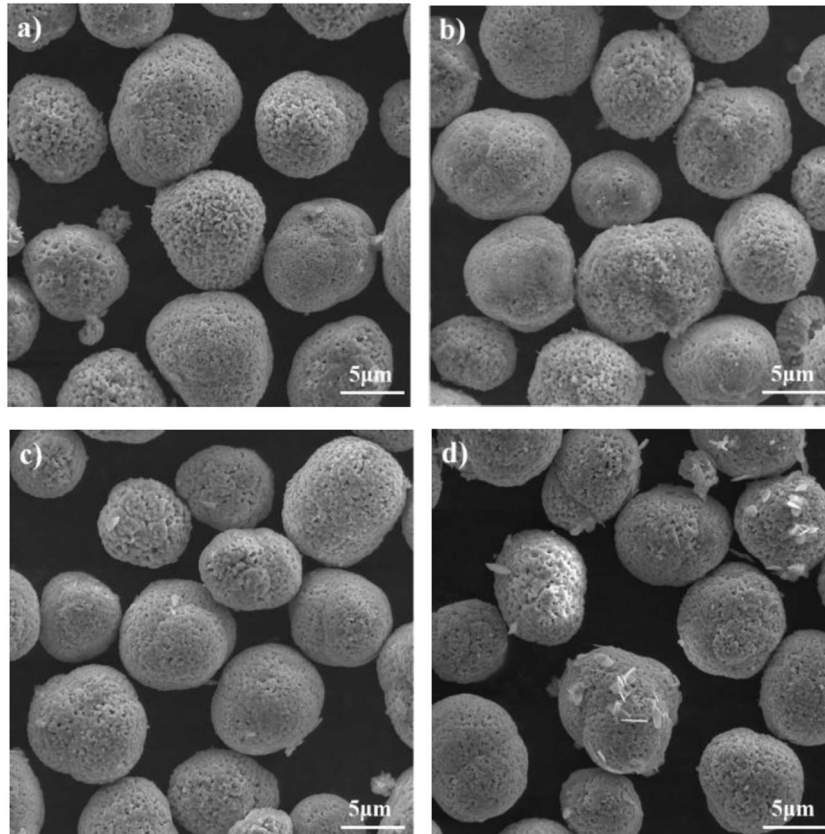
**Fig. 3** TEM image of LR-NMC@0.03 Li-rich cathode

in XRD pattern shown in Fig. 1 after La doping, it can be concluded that  $\text{La}^{3+}$  ions that are not fully doped into the layered structure of the lithium-rich cathode material exist on the surface of the material particles in the form of

$\text{LaMnO}_3$ . In order to better identify the existence details of  $\text{LaMnO}_3$  phase on the particle surface, TEM characterization was adopted to analysis morphology and coating situation of  $\text{LaMnO}_3$  phase. The coating layer of about 2–3 nm shown in Fig. 3 can be clearly seen on the surface of the LR-NMC@0.03 Li-rich cathode particle. Meanwhile, the coating layer on the particle surface is dense and uniform. According to the phase analysis result in Fig. 1 and the EDS test result in Fig. 2b and d, the coating layer can be determined as  $\text{LaMnO}_3$ .

SEM was adopted to analyze the morphology and particle size of the pristine and the  $\text{La}^{3+}$  modified samples. Figure 4 presents the SEM images of the Pristine and the  $\text{La}^{3+}$  modified samples. As shown in Fig. 4, all the samples with the particle size about  $10\ \mu\text{m}$  are secondary particles formed by stacking primary particles, and the particles are dispersed evenly. The samples still maintain good spherical morphology after modified by  $\text{La}^{3+}$  ion. It is noteworthy that the surface of  $\text{La}^{3+}$  modified samples is more smooth and compact. However, the surface of the pristine sample is coarse, and there are many randomly distributed holes on the surface. Figure 5 presents the EDS mapping patterns of LR-NMC@0.03 Li-rich cathodes. As shown in Fig. 5, Ni, Co, Mn, and La elements were detected successfully on the particle surface by the EDS test. Meanwhile, all the detected elements distribute uniformly. The La element that distributes

**Fig. 4** SEM images of  $\text{Li}_{1.2}\text{Mn}_{0.54-x}\text{Ni}_{0.13}\text{Co}_{0.13}\text{La}_x\text{O}_2$  ( $x = 0, 0.01, 0.03, 0.05$ ) Li-rich cathodes: **a**  $x = 0$ , **b**  $x = 0.01$ , **c**  $x = 0.03$ , and **d**  $x = 0.05$



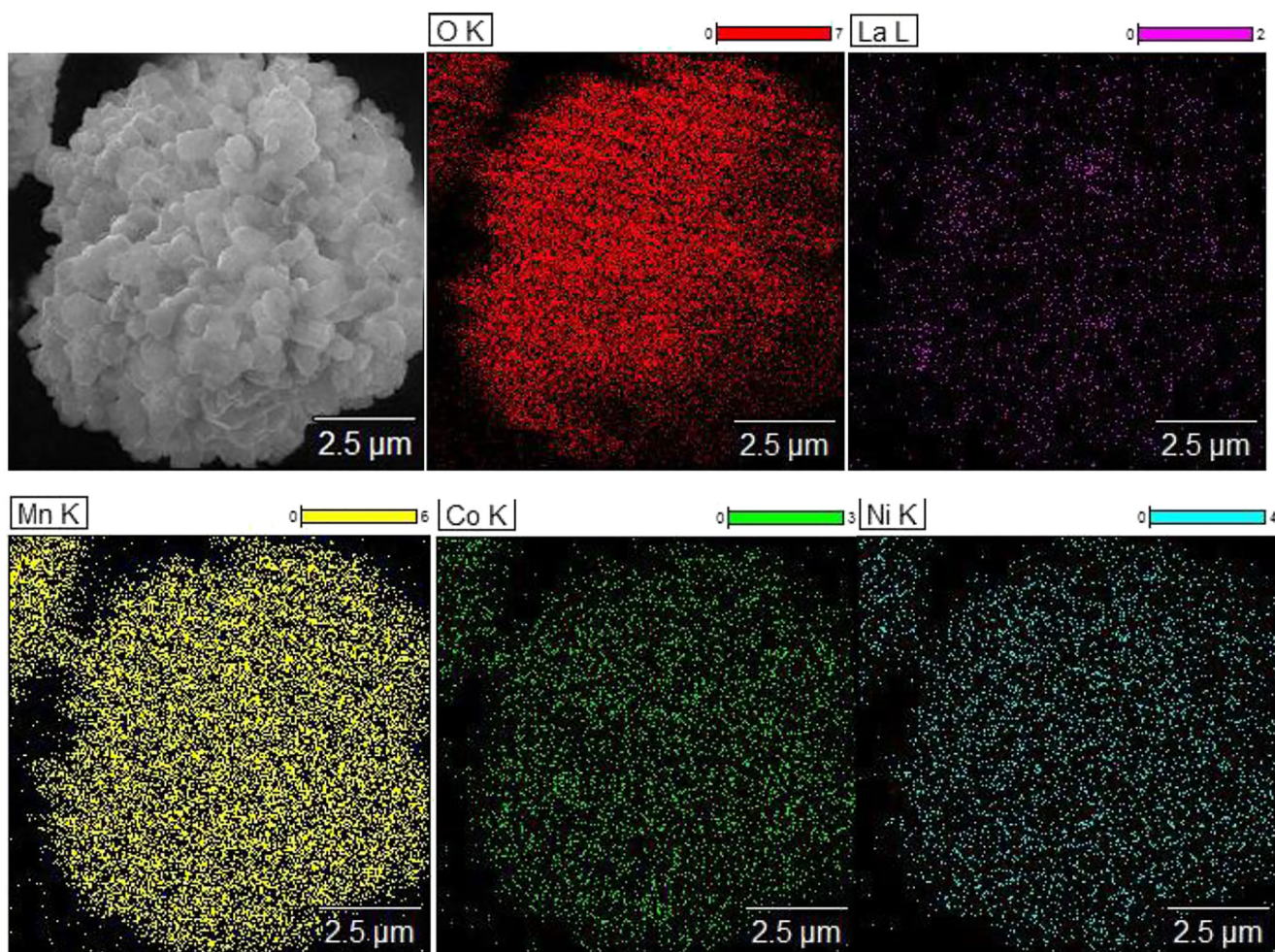


Fig. 5 EDS mapping patterns of LR-NMC@0.03 Li-rich cathodes

uniformly can be considered that  $\text{LaMnO}_3$  coating layer is well coated on the surface of positive particles. This result is well in accord with the analysis in Fig. 3.

The charge-discharge profiles of  $\text{Li}_{1.2}\text{Mn}_{0.54-x}\text{Ni}_{0.13}\text{Co}_{0.13}\text{La}_x\text{O}_2$  ( $x = 0, 0.01, 0.03, 0.05$ ) Li-rich cathodes in the first cycle conducted from 2.0 V to 4.6 V at C/10 ( $1C = 250 \text{ mA g}^{-1}$ ) are shown in Fig. 6. All the samples exhibit similar charge-discharge curve characteristics, i.e., the charge profiles of all the samples consist of a slant line below 4.5 V and a plateau around 4.5 V, corresponding to the oxidation of nickel and cobalt and the activation of  $\text{Li}_2\text{MnO}_3$ , respectively [34–36]. The charge-discharge capacity values, the irreversible capacity (Cirr) values, and the coulombic efficiency for all the samples in the first cycle are listed in Table 2. With the increase of La doping content, the charge capacity of the sample decreases in turn; however, the discharge capacity of the sample increases first and then decreases. It is important to note that the initial discharge capacity of  $\text{Li}_{1.2}\text{Mn}_{0.54-x}\text{Ni}_{0.13}\text{Co}_{0.13}\text{La}_x\text{O}_2$  when  $x = 0.03$  can reach as high as  $286.7 \text{ mAh g}^{-1}$  compared with that of  $260.6 \text{ mAh g}^{-1}$  for the pristine sample ( $x = 0$ ). Furthermore, the Cirr value

reduces from  $77.0$  to  $36.4 \text{ mAh g}^{-1}$ , and the initial coulombic efficiency also increases from  $77.2$  to  $88.7\%$ . Appropriate La doping cannot only broaden the transport channel of lithium-

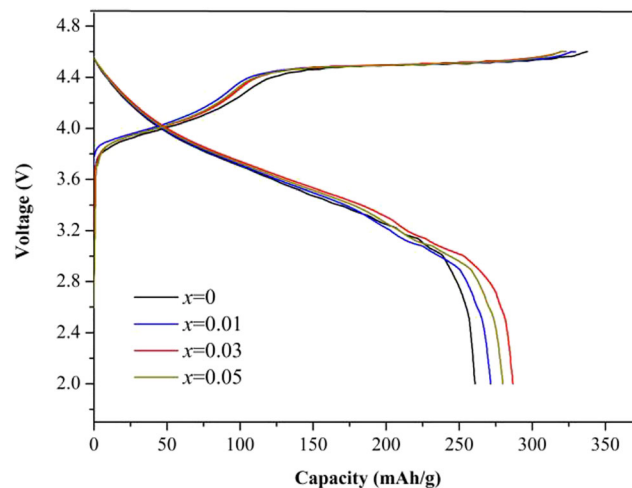


Fig. 6 The initial charge-discharge curves of LR-NMC@0.03 Li-rich cathodes in 2.0–4.6 V at C/10

**Table 2** The initial charge-discharge data of  $\text{Li}_{1.2}\text{Mn}_{0.54-x}\text{Ni}_{0.13}\text{Co}_{0.13}\text{La}_x\text{O}_2$  ( $x = 0, 0.01, 0.03, 0.05$ ) Li-rich cathodes

Sample ( $x$ )	First charge capacity/ $\text{mAh g}^{-1}$	First discharge capacity/ $\text{mAh g}^{-1}$	Irreversible capacity/ $\text{mAh g}^{-1}$	First coulomb efficiency/%
0.00	337.6	260.6	77.0	77.2
0.01	329.7	271.5	58.2	82.3
0.03	323.1	286.7	36.4	88.7
0.05	321.8	279.3	42.5	86.8

ion but also stabilize the structure of the material.  $\text{LaMnO}_3$  formed by La that has not entered the material structure was coated on the surface of the material which can effectively prevent the electrolyte from eroding the surface of the cathode electrode material. Meanwhile, the  $\text{LaMnO}_3$  coating layer can protect oxygen vacancies generated during the first charge and suppress the evolution of  $\text{O}_2$  gas to a certain extent [27, 37]. Thus the discharge performance of the lithium-rich cathode material has been effectively improved. However, too little doping of La has limited effect on improving the structure and electrochemical performance of the material. Excessive doping of 'La<sup>3+</sup>' does not completely allow 'La<sup>3+</sup>' to enter the lattice of the layered material and generates too much two-phase  $\text{LaMnO}_3$ . The excessive  $\text{LaMnO}_3$  may hinder the transport of lithium-ions, which worsens the electrochemical properties of the cathode material.

To evaluate the rate performance of the 'La<sup>3+</sup>' modified samples, the rate capacity voltage of the pristine for Fig. 7a and LR-NMC@0.03 for Fig. 7b at C/10, C/5, C/2, 1C, and 2C had been conducted. It can be seen that the LR-NMC@0.03 sample delivers a higher discharge capacity than that of the pristine at all the tested rates. For instance, LR-NMC@0.03 sample exhibits a discharge capacity of  $248.1 \text{ mAh g}^{-1}$  at 1C in comparison with that of  $212.3 \text{ mAh g}^{-1}$  for the pristine. Interestingly, all the spacing between adjacent capacity-voltage curves for the LR-NMC@0.03 sample are narrower than those of the pristine. The above analysis indicates that the LR-NMC@0.03 sample has a better rate performance.

To establish better understanding of the origin of the better rate capability for the LR-NMC@0.03 sample, the differential capacity versus voltage ( $dQ/dV$ ) plotted in Fig. 8 had been performed at 1C rate for both the pristine sample and the LR-NMC@0.03 sample. As we know, the origin of the redox species comes from  $\text{Ni}^{2+} \leftrightarrow \text{Ni}^{3+} \leftrightarrow \text{Ni}^{4+}$  and  $\text{Co}^{3+} \leftrightarrow \text{Co}^{4+}$  oxidation/reduction reaction simultaneously accompanied with different phase transitions during the electrochemical processes as reported in the researches [38–40]. The two obvious reduction peaks displayed in Fig. 8 shift to higher potential in the LR-NMC@0.03 sample compared with that in the pristine sample. Previous study [40] shows that the peak potential is closely related to the total polarization of the experimental samples including ohmic polarization, charge transfer polarization, and diffusion polarization. Specifically, the higher the peak potential value, the smaller the total polarization value, which is under the discharge process of cathode electrode. In other words, the LR-NMC@0.03 sample possesses higher the peak potential value than the pristine, indicating lower total polarization value. Therefore, the LR-NMC@0.03 sample exhibits better rate capability.

To further clarify the origin of the enhanced rate capability for the LR-NMC@0.03 sample comprising the pristine sample, electrochemical impedance spectra (EIS) measurement had been conducted at 25 °C after the first cycle and 100 cycles. All the samples were charged to 4.6 V at 1C before tested. The inset is the equivalent circuit used to fit the Nyquist plots listed in Fig. 9. In general, a Nyquist plot

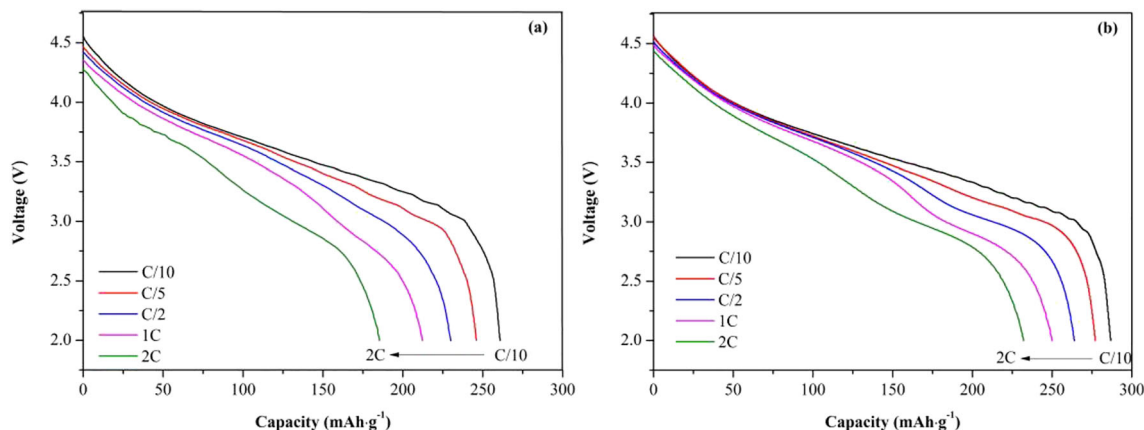


**Fig. 7** The rate performances of  $\text{Li}_{1.2}\text{Mn}_{0.54-x}\text{Ni}_{0.13}\text{Co}_{0.13}\text{La}_x\text{O}_2$  Li-rich cathodes for **a**  $x = 0$  and **b**  $x = 0.03$

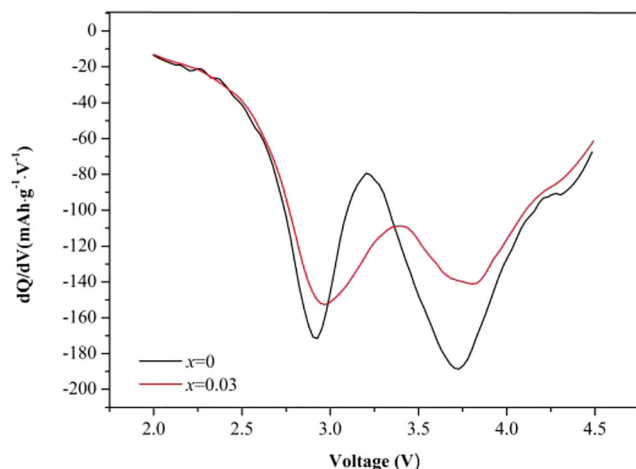


**Fig. 8** The  $dQ/dV$  curves of the discharge process at 1C rate of the pristine sample and LR-NMC@0.03 sample

for the lithium-rich cathode material consists of two semicircles and one slope. Specifically, the intercept of the first semicircle with real axis in the highest frequency region represents the ohmic resistance ( $R_s$ ) of electrolyte, separator, and electrode. The first semicircle in the high frequency region and the second semicircle in the middle frequency region refer to the resistance ( $R_f$ ) of lithium-ion diffusion in the solid-electrolyte interface (SEI) and the charge transfer resistance ( $R_{ct}$ ) in the electrode and electrolyte interface, respectively. The slope in the low frequency region belongs to Warburg impedance ( $W_o$ ) of lithium-ion diffusion in the bulk electrodes [41]. In this study, each Nyquist plot of both the samples exhibit an overlapped semicircle in the high-to-medium frequency region and a slope straight line in the low frequency region. It should be pointed that the semicircle of the high frequency region can be mainly attributed to the  $R_{ct}$ . Generally, the  $R_s$  for the cathode materials is far less than the  $R_{ct}$ . As shown in Fig. 9, the charge transfer resistance ( $R_{ct}$ ) values of both the samples no

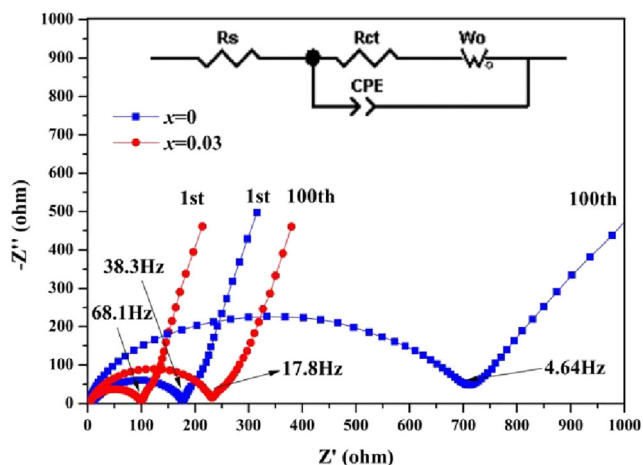


**Fig. 9** Nyquist plots of  $\text{Li}_{1.2}\text{Mn}_{0.54-x}\text{Ni}_{0.13}\text{Co}_{0.13}\text{La}_x\text{O}_2$  Li-rich cathodes at 1st and 100th cycles

**Table 3** The fitting data of  $R_s$  and  $R_{ct}$  of  $\text{Li}_{1.2}\text{Mn}_{0.54-x}\text{Ni}_{0.13}\text{Co}_{0.13}\text{La}_x\text{O}_2$  Li-rich cathodes for (a)  $x=0$  and (b)  $x=0.03$  at the 1st and 100th cycle

Sample ( $x$ )	Cycle	$R_s$ ( $\Omega$ )	$R_{ct}$ ( $\Omega$ )
0.00	1st	4.1	177.8
	100th	5.8	713.9
0.03	1st	3.2	98.7
	100th	4.7	226.2

matter in which cycle have contributed the main part of the total impedance. However, the ohmic resistance ( $R_s$ ) values as a tiny part of the total impedance are less than  $6 \Omega$ . Furthermore, there is very little difference in the  $R_s$  values between the pristine samples and the LR-NMC@0.03 samples, indicating that the modification of  $\text{La}^{3+}$  does not change the conductivity of the cathode electrode material. The details of the fitting impedance data are recorded in Table 3. It's remarkable that the  $R_{ct}$  values for the pristine sample at the 1st and 100th cycle are both greater than that of the LR-NMC@0.03 sample. Moreover, the  $R_{ct}$  values for the pristine sample increase from  $177.8 \Omega$  at the 1st cycle to  $713.9 \Omega$  at the 100th cycle, while the  $R_{ct}$  values for the LR-NMC@0.03 sample increase from  $98.7 \Omega$  at the 1st cycle to  $226.2 \Omega$  at the 100th cycle. The lower  $R_{ct}$  values for the LR-NMC@0.03 sample at the 1st and 100th cycle can be ascribed to the effective inhibition of side reaction on the cathode/electrolyte interface by the  $\text{LaMnO}_3$  coating. Previous research results [42, 43] show that the dominant factor of the rate performance for the cathode electrode materials was the  $R_{ct}$  value. Specifically, the electrode polarization decreases with the decrease of the  $R_{ct}$  value, resulting in a better rate performance. It is worth mentioning that  $\text{La}^{3+}$  doping can effectively broaden the lithium-ion channel in the lattice as shown in Table 1 and further facilitates the transport of lithium-ions, thus improving the

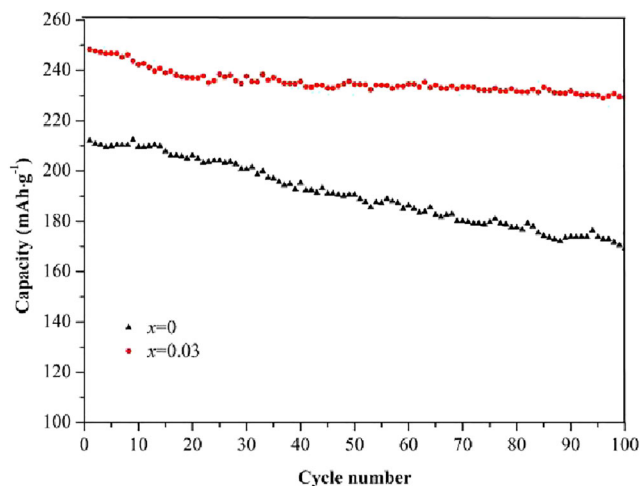


**Fig. 10** Cycling performance of  $\text{Li}_{1.2}\text{Mn}_{0.54-x}\text{Ni}_{0.13}\text{Co}_{0.13}\text{La}_x\text{O}_2$  Li-rich cathodes in 2.0–4.6 V at 1C



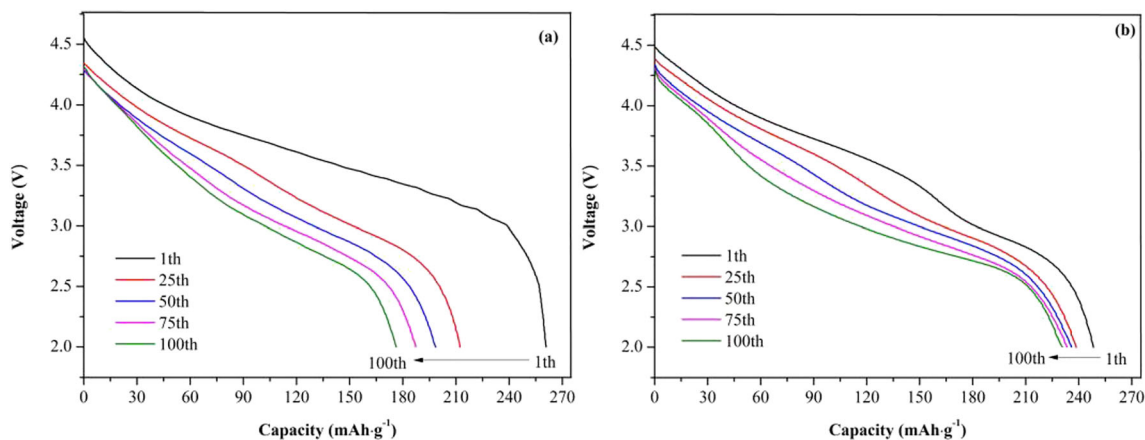


**Fig. 11** Cyclic discharge curves of  $\text{Li}_{1.2}\text{Mn}_{0.54-x}\text{Ni}_{0.13}\text{Co}_{0.13}\text{La}_x\text{O}_2$  Li-rich cathodes for **a**  $x = 0$  and **b**  $x = 0.03$

rate performance of the 'La<sup>3+</sup>' modified sample. Overall, the double strengthening effect of the 'La<sup>3+</sup>' modification promotes the LR-NMC@0.03 sample's own better rate capability.

To evaluate the cycling stability of the pristine sample and the LR-NMC@0.03 sample, the charge-discharge cycle test had been performed at 1C with the potential window of 2.0–4.6 V. Figure 10 presents the details with regard to the relation between the cycle number and discharge capacity for both the pristine sample and the 'La<sup>3+</sup>' modified sample. The pristine sample delivers an initial discharge capacity and the discharge capacity after 100 cycles of 212.3 mAh g<sup>-1</sup> and 163.1 mAh g<sup>-1</sup>, respectively, the discharge capacity retention of which is only 76.8%. Interestingly, the discharge capacity retention of LR-NMC@0.03 sample can reach 92.5%, corresponding to the initial discharge capacity is 248.1 mAh g<sup>-1</sup> and the 100th cycle discharge capacity is 229.4 mAh g<sup>-1</sup>. The cyclic discharge curves at 1st, 25th, 50th, 75th, and 100th for both the samples are plotted in Fig. 11. It can be clearly seen that the discharge curves of the LR-NMC@0.03 sample at different cycles are noticeably denser compared with those of the pristine samples, indicating a lower capacity decay rate. The better cyclic stability of the LR-NMC@0.03 sample can be ascribed to the more stable host structure and surface structure for the double strengthening effect by both the 'La<sup>3+</sup>' doping and LaMnO<sub>3</sub> coating. Firstly, the 'La<sup>3+</sup>' doping makes the cathode electrode material own a better layered structure. And the mixed arrangement degree of Li<sup>+</sup> and Ni<sup>2+</sup> cations has been lowered as analyzed in the second paragraph of the "Results and discussions" section. In addition, the binding energy of La–O bond is higher than that of Ni–O or Mn–O bond as described in the fourth paragraph of the "Introduction" section, which helps to retain oxygen vacancies in the structure of the cathode material and further improve the structure stability. Secondly, the LaMnO<sub>3</sub> coating layer can suppress the corrosion of the cathode electrode material by the electrolyte, preventing the surface structure of the cathode electrode from severe collapse. Actually, one can find

that the Rct value of the LR-NMC@0.03 sample only increases from 98.7 Ω at the 1st cycle to 226.2 Ω at the 100th cycle compared with that of the pristine; thus, the slow increase in Rct values during long cycles for the LaMnO<sub>3</sub> coating facilitates the migration of lithium-ions across the cathode/electrolyte interface.

### Conclusions

The one-step method for 'La<sup>3+</sup>' doping and LaMnO<sub>3</sub> coating is successfully applied to modify the  $\text{Li}_{1.2}\text{Mn}_{0.54}\text{Ni}_{0.13}\text{Co}_{0.13}\text{O}_2$  cathode material. The electrochemical performances of the  $\text{Li}_{1.2}\text{Mn}_{0.54}\text{Ni}_{0.13}\text{Co}_{0.13}\text{O}_2$  for the double strengthening effect by 'La<sup>3+</sup>' doping and LaMnO<sub>3</sub> coating had been improved effectively. The LR-NMC@0.03 sample exhibits lower irreversible capacity loss, higher initial coulomb efficiency, higher discharge capacity, better cyclic performance, and better rate capability compared with those of the pristine sample. The better electrochemical properties for the LR-NMC@0.03 sample can be attributed to stability improvement of its host structure and surface structure by 'La<sup>3+</sup>' doping and LaMnO<sub>3</sub> coating, respectively. It is worth mentioning that one-step method by the 'La<sup>3+</sup>' modified can be extended to other kinds of cathode materials.

**Funding information** This work was supported by the Science and Technology Program of Sichuan Province under grant number 2019YJ0539.

### References

1. Tarascon JM, Armand M (2001) Issues and challenges facing rechargeable lithium. *Nature* 414:359–367
2. Armand M, Tarascon JM (2008) Building better batteries. *Nature* 451:652–657

3. Melot BC, Tarascon JM (2013) Design and preparation of materials for advanced electrochemical storage. *Acc Chem Res* 46:1226–1238
4. Larcher D, Tarascon JM (2015) Towards greener and more sustainable batteries for electrical energy storage. *Nat Chem* 7:19–29
5. Xu B, Qian D, Wang ZY, Meng YS (2012) Recent progress in cathode materials research for advanced lithium ion batteries. *Mater Sci Eng R* 73:51–65
6. Yao X, Xua Z, Yao Z, Chenga W, Gaob H, Zhaoa Q, Lia J, Zhoua A (2019) Oxalate co-precipitation synthesis of  $\text{LiNi}_{0.6}\text{Co}_{0.2}\text{Mn}_{0.2}\text{O}_2$  for low-cost and high-energy lithium-ion batteries. *Mater Today Commun* 19:262–270
7. Chen S, He T, Su YF, Lu Y, Ban LY, Chen L, Zhang QY, Wang J, Chen RJ, Wu F (2017) Ni-rich  $\text{LiNi}_{0.8}\text{Co}_{0.1}\text{Mn}_{0.1}\text{O}_2$  oxide coated by dual-conductive layers as high performance cathode for lithium-ion batteries. *ACS Appl Mater Interfaces* 9:29732–29743
8. Tsai YW, Hwang BJ, Ceder G (2005) In-situ x-ray absorption spectroscopic study on variation of electronic transitions and local structure of  $\text{LiNi}_{1/3}\text{Co}_{1/3}\text{Mn}_{1/3}\text{O}_2$  cathode material during electrochemical cycling. *Chem Rev* 17(12):3191–3199
9. Wu F, Wang M, Su YF (2009) Effect of  $\text{TiO}_2$ -coating on the electrochemical performances of  $\text{LiCo}_{1/3}\text{Ni}_{1/3}\text{Mn}_{1/3}\text{O}_2$ . *J Power Sources* 191(2):628–632
10. Liu W, Li X, Xiong D, Hao Y, Li J, Kou H, Yan B, Li D, Lu S, Koo A, Adair K, Sun X (2018) Significantly improving cycling performance of cathodes in lithium ion batteries: the effect of  $\text{Al}_2\text{O}_3$  and  $\text{LiAlO}_2$  coatings on  $\text{LiNi}_{0.6}\text{Co}_{0.2}\text{Mn}_{0.2}\text{O}_2$ . *Nano Energy* 44:111–120
11. Xie HM, Wang RS, Ying JR, Zhang LY, Jalbout AF, Yu HY, Yang GL, Pan XM, Su ZM (2006) Optimized  $\text{LiFePO}_4$ -polyacene cathode material for lithium-ion batteries. *Adv Mater* 18(19):2609–2613
12. Wang Y, Wang Y, Hosono E, Wang K, Zhou H (2008) The design of a  $\text{LiFePO}_4$ /carbon nanocomposite with a core-shell structure and its synthesis by an in situ polymerization restriction method. *Angew Chem Int Ed* 47:7461–7465
13. Kim DK, Muralidharan P, Lee HW, Ruffo R, Yang Y, Chan CK, Peng HL, Huggins RA, Cui Y (2008) Spinel  $\text{LiMn}_2\text{O}_4$  nanorods as lithium ion battery cathodes. *Nano Lett* 11:3948–3952
14. Hosono E, Kudo T, Honma I, Matsuda H, Zhou HS (2009) Synthesis of single crystalline spinel  $\text{LiMn}_2\text{O}_4$  nanowires for a lithium ion battery with high power density. *Nano Lett* 3:1045–1051
15. Liu H, Chen C, Du C et al (2015) Lithium-rich  $\text{Li}_{1.2}\text{Ni}_{0.13}\text{Co}_{0.13}\text{Mn}_{0.54}\text{O}_2$  oxide coated by  $\text{Li}_3\text{PO}_4$  and carbon nanocomposite layers as high performance cathode materials for lithium ion batteries. *J Mater Chem A* 3:2634–2641
16. Li B, Yan H, Ma J, Yu P, Xia D, Huang W, Chu W, Wu Z (2014) Manipulating the electronic structure of Li-rich manganese-based oxide using polyanions: towards better electrochemical performance. *Adv Funct Mater* 24:5112–5118
17. Nayak PK, Grinblat J, Levi M, Levi E, Kim S, Choi JW, Aurbach D (2016) Al doping for mitigating the capacity fading and voltage decay of layered Li and Mn-rich cathodes for Li-ion batteries. *Adv Energy Mater* 6:1502398
18. Iddir H, Benedek R (2014) First-principles analysis of phase stability in layered-layered composite cathodes for lithium-ion batteries. *Chem Mater* 26:2407–2413
19. Park YJ, Hong YS, Chang SH (2004) Structural investigation and electrochemical behaviour of  $\text{Li}[\text{Ni}_x\text{Li}_{1/3-2x/3}\text{Mn}_{2/3-x/3}]\text{O}_2$  compounds by a simple combustion method. *J Power Sources* 129: 288–295
20. Yabuuchi N, Yoshii K, Myung ST, Nakai I, Komaba S (2011) Detailed studies of a high-capacity electrode material for rechargeable batteries,  $\text{Li}_2\text{MnO}_3$ - $\text{LiCo}_{1/3}\text{Ni}_{1/3}\text{Mn}_{1/3}\text{O}_2$ . *J Am Chem Soc* 133:4404–4419
21. Lee CW, Sun YK, Prakash J (2004) A novel layered  $\text{Li}[\text{Li}_{0.12}\text{Ni}_x\text{Mg}_{0.32-2x}\text{Mn}_{0.56}]\text{O}_2$  cathode material for lithium-ion batteries. *Electrochim Acta* 49:4425–4432
22. Park SH, Sun YK (2003) Synthesis and electrochemical properties of layered  $\text{Li}[\text{Li}_{0.15}\text{Ni}_{(0.275-x/2)}\text{Al}_x\text{Mn}_{(0.575-x/2)}]\text{O}_2$  materials prepared by sol-gel method. *J Power Sources* 119:161–165
23. Park C, Kim S, Nahm K et al (2008) Structural and electrochemical study of  $\text{Li}[\text{Cr}_x\text{Li}_{(1-x)/3}\text{Mn}_{2(1-x)/3}]\text{O}_2$  ( $0 \leq x \leq 0.328$ ) cathode materials. *J Alloys Compd* 449:343–348
24. Zhang XF, Belharouak I, Li L, Lei Y, Elam JW, Nie A, Chen XQ, Yassar RS, Axelbaum RL (2013) Structural and electrochemical study of  $\text{Al}_2\text{O}_3$  and  $\text{TiO}_2$  coated  $\text{Li}_{1.2}\text{Ni}_{0.13}\text{Mn}_{0.54}\text{Co}_{0.13}\text{O}_2$  cathode material using ALD. *Adv Energy Mater* 3(10):1209–1307
25. Kong JZ, Zhai HF, Qian X, Wang M, Wang QZ, Li AD, Li H, Zhou F (2017) Improved electrochemical performance of  $\text{Li}_{1.2}\text{Mn}_{0.54}\text{Ni}_{0.13}\text{Co}_{0.13}\text{O}_2$  cathode material coated with ultrathin  $\text{ZnO}$ . *J Alloys Compd* 694:848–854
26. Wang ZY, Liu EZ, Guo LC, Shi CS, He CN, Li JJ, Zhao NQ (2013) Cycle performance improvement of Li-rich layered cathode material  $\text{Li}[\text{Li}_{0.2}\text{Mn}_{0.54}\text{Ni}_{0.13}\text{Co}_{0.13}]\text{O}_2$  by  $\text{ZrO}_2$  coating. *Surf Coat Technol* 235:570–576
27. Qiu B, Zhang MH, Wu LJ, Wang J, Xia YG, Qian DN, Liu HD, Hy S, Chen Y, An K, Zhu YM, Liu ZP, Meng YS (2016) Gas-solid interfacial modification of oxygen activity in layered oxide cathodes for lithium-ion batteries. *Nat Commun* 7:12108
28. Speight JG (2005) Lange's handbook of chemistry [M]. Mc Graw-Hill, New York
29. Deng H, Belharouak I, Sun YK (2009)  $\text{Li}_x\text{Ni}_{0.25}\text{Mn}_{0.75}\text{O}_y$  ( $0.5 \leq x \leq 2.2$ ,  $y \leq 2.75$ ) compounds for high-energy lithium-ion batteries. *J Mater Chem* 19(26):4510–4516
30. Jarvis KA, Deng Z, Allard LF (2011) Atomic structure of a lithium-rich layered oxide material for lithium-ion batteries: evidence of a solid solution. *J Mater Chem* 23(16):3614–3621
31. Myungs T, Izumi K, Komaba S (2005) Role of alumina coating on Li-Ni-Co-Mn-O particles as positive electrode material for lithium-ion batteries. *J Mater Chem* 17(14):3695–3704
32. Ding Y, Zhang P, Jiang Y (2007) Effect of rare earth elements doping on structure and electrochemical properties of  $\text{LiNi}_{1/3}\text{Co}_{1/3}\text{Mn}_{1/3}\text{O}$  for lithium-ion battery. *Solid State Ionics* 178:967–971
33. Li N, An R, Su YF (2013) The role of yttrium content in improving electrochemical performance of layered lithium-rich cathode materials for Li-ion batteries. *J Mater Chem A* 1:9760–9767
34. Arunkumar TA, Wu Y, Manthiram A (2007) Factors influencing the irreversible oxygen loss and reversible capacity in layered  $\text{Li}[\text{Li}_{1/3}\text{Mn}_{2/3}]\text{O}_2$ - $\text{Li}[\text{M}]\text{O}_2$  ( $\text{M}=\text{Mn}_{0.5-x}\text{Ni}_{0.5-x}\text{Co}_{2x}$  and  $\text{Ni}_{1-x}\text{Co}_x$ ) solid solutions. *Chem Mater* 19:3067–3073
35. Wu Y, Manthiram A (2006) High capacity, surface-modified layered  $\text{Li}[\text{Li}_{(1-x)/3}\text{Mn}_{(2-x)/3}\text{Ni}_{1/3}\text{Co}_{x/3}]\text{O}_2$  cathodes with low irreversible capacity loss. *Electrochem. Solid-State Lett* 9: A221–A224
36. Liu W et al (2015) Countering voltage decay and capacity fading of lithium-rich cathode material at 60C by hybrid surface protection layers. *Adv Energy Mater* 5:201500274
37. Florian S, Hana B, Mudit D et al (2017) From surface  $\text{ZrO}_2$  coating to bulk Zr doping by high temperature annealing of nickel-rich lithiated oxides and their enhanced electrochemical performance in lithium ion batteries. *Adv Energy Mater* 7:1701682
38. Ghanty C, Markovsky B, Erickson EM et al (2015)  $\text{Li}^+$ -ion extraction/insertion of Ni-rich  $\text{Li}_{1+x}(\text{Ni}_y\text{Co}_z\text{Mn}_z)_w\text{O}_2$  ( $0.005 < x < 0.03$ ;  $y:z=8:1$ ,  $w \approx 1$ ) electrodes: in situ XRD and Raman spectroscopy study. *ChemElectroChem* 2:1479
39. Li J, Downie LE, Ma L, Qiu W, Dahn J (2015) Study of the failure mechanisms of  $\text{LiNi}_{0.8}\text{Mn}_{0.1}\text{Co}_{0.1}\text{O}_2$  cathode material for Lithium ion batteries. *J Electrochem Soc* 162:A1401

40. Liu J, Yang Y, Yu P, Li Y, Shao H (2006) Electrochemical characterization of  $\text{LaNi}_{5-x}\text{Al}_x$  ( $x=0.1-0.5$ ) in the absence of additives. *J Power Sources* 161:1435
41. Tan KS, Reddy MV, Subba GV, Chowdari BV (2005) Effect of  $\text{AlPO}_4$ -coating on cathodic behaviour of  $\text{Li}(\text{Ni}_{0.8}\text{Co}_{0.2})\text{O}_2$ . *J Power Sources* 141:129
42. Jafta CJ, Ozoemena KI, Mathe MK, Roos WD (2012) Synthesis, characterisation and electrochemical intercalation kinetics of nanostructured aluminium-doped  $\text{Li}[\text{Li}_{0.2}\text{Mn}_{0.54}\text{Ni}_{0.13}\text{Co}_{0.13}]\text{O}_2$  cathode material for lithium ion battery. *Electrochim Acta* 85:411–422
43. Liu J, Jayan BR, Manthiram A (2010) Conductive surface modification with aluminum of high capacity layered  $\text{Li}[\text{Li}_{0.2}\text{Mn}_{0.54}\text{Ni}_{0.13}\text{Co}_{0.13}]\text{O}_2$  cathodes. *J Phys Chem C* 114:9528–9533

**Publisher's note** Springer Nature remains neutral with regard to jurisdictional claims in published maps and institutional affiliations.